European Journal of Pharmaceutics and Biopharmaceutics 194 (2024) 49–61

Contents lists available at ScienceDirect

European Journal of Pharmaceutics and Biopharmaceutics

journal homepage: www.elsevier.com/locate/ejpb

Research paper

Rapid liposomal formulation for nucleolin targeting to rhabdomyosarcoma cells

Dzhangar Dzhumashev [a,b,c], Stenija Anton-Joseph [a,b,c,1], Victoria J. Morel [a,b,1], Andrea Timpanaro [a,b,c], Gregor Bordon [d], Caroline Piccand [a,b,c], Simone Aleandri [d], Paola Luciani [d], Jochen Rössler [a,b], Michele Bernasconi [a,b,*]

[a] Department of Pediatric Hematology and Oncology, Inselspital, Bern University Hospital, 3010 Bern, Switzerland
[b] Department for BioMedical Research (DBMR), University of Bern, 3008 Bern, Switzerland
[c] Graduate School for Cellular and Biomedical Sciences, University of Bern, 3012 Bern, Switzerland
[d] Department of Chemistry, Biochemistry and Pharmaceutical Sciences, University of Bern, 3012 Bern, Switzerland

ARTICLE INFO

Keywords:
Targeted drug delivery
Liposomes
Rhabdomyosarcoma
Nucleolin
Vincristine
F3 peptide

ABSTRACT

Rhabdomyosarcoma (RMS) is the most common pediatric soft tissue sarcoma. More effective and less toxic therapies are urgently needed for high-risk patients. Peptide-guided targeted drug delivery can increase the therapeutic index of encapsulated drugs and improve patients' well-being. To apply this strategy to RMS, we identified the peptide F3 in a screening for peptides binding to RMS cells surface. F3 binds to nucleolin, which is present on the surface of RMS cells and is abundantly expressed at the mRNA level in RMS patients' biopsies compared to healthy tissues. We developed a rapid microfluidic formulation of F3-decorated PEGylated liposomes and remote loading of the chemotherapeutic drug vincristine. Size, surface charge, drug loading and retention of targeted and control liposomes were studied. Enhanced cellular binding and uptake were observed in three different nucleolin-positive RMS cell lines. Importantly, F3-functionalized liposomes loaded with vincristine were up to 11 times more cytotoxic than non-targeted liposomes for RMS cell lines. These results demonstrate that F3-functionalized liposomes are promising for targeted drug delivery to RMS and warrant further *in vivo* investigations.

1. Introduction

1.1. Rhabdomyosarcoma

Rhabdomyosarcoma (RMS) is the most common soft tissue sarcoma and accounts for more than half of soft tissue sarcomas in pediatric patients [1]. Histology separates four major subtypes: embryonic RMS (eRMS) and alveolar RMS (aRMS) account respectively for 60–70 % and 20–30 % of all cases whereas pleomorphic (pRMS) and spindle cell/sclerosing (s-scRMS) account for 7–15 % of the cases [2]. The aggressive aRMS tumors carry one of two characteristic chromosomal translocations, t(2;13)(q35;q14) or t(1;13)(p36;q14) that result in the expression of PAX3-FOXO1 or PAX7-FOXO1 fusion transcription factor, respectively [3], and are therefore now classified as fusion-positive (FP) RMS. Embryonal RMS tumors have a better prognosis and are clinically indistinguishable from fusion-negative (FN) RMS [4]. Surgery, chemotherapy, and radiotherapy are the main therapeutic approaches to treat local and metastatic disease. Prior to the introduction of multi-agent therapy in 1969, the overall survival was less than 25 %, and over the past four decades it has improved significantly reaching up to 70 % [5].

Today, the standard systemic chemotherapy administered consists in a combination of vincristine (VCR), actinomycin-D, and cyclophosphamide in the VAC regimen [6,7]; cyclophosphamide can be substituted by ifosfamide in the VAI regimen [8]. Especially metastatic RMS still has a bad prognosis with very low survival rates [9]. The current treatments are highly aggressive and can cause lifelong debilitating side effects. One of the chemotherapeutics widely used is VCR, which is known to cause severe peripheral neuropathy as acute and long-term toxicity. The quality of life of children under treatment [10], as of survivors [11] is therefore significantly affected.

* Corresponding author at: Department of Pediatric Hematology and Oncology, Inselspital, Bern University Hospital, 3010 Bern, Switzerland.
E-mail address: michele.bernasconi@unibe.ch (M. Bernasconi).
[1] Contributed equally.

https://doi.org/10.1016/j.ejpb.2023.11.020
Received 31 August 2023; Received in revised form 20 November 2023; Accepted 23 November 2023
Available online 27 November 2023

Increase of therapeutic response and reduction of side effects has been realized by using drug carriers for selective uptake [12]. Multiple technologies have been applied in nanoparticles delivery platforms, such as liposomes [13], polymeric [14], and inorganic nanoparticles [15]. Several of these have reached the clinical testing phase also for pediatric tumors [16]. In 1995, the liposomal formulations of doxorubicin Doxil®, coated with polyethylene glycol (PEG) [17], and the non-PEGylated Myocet® [18], were the first cancer nanomedicines to be approved by the FDA. Both drugs achieved a lower toxicity profile and improved efficacy compared to the free drug. In 2012, VCR sulfate liposome injection, Marqibo®, a non-PEGylated liposomal formulation of VCR, was granted accelerated approval by the FDA for relapsed acute lymphoblastic leukemia [19]. Interestingly, the tolerability of Marqibo® in pediatric patients, including one patient with RMS, was acceptable within the applied dose (Phase I trial, NCT01222780) [20]. We previously have reported prolonged circulation and increased tumor accumulation of VCR loaded into sphingomyelin/cholesterol-based liposomes, formulation similar to Marqibo®, modified with PEG groups [21].

Active targeting by surface modification of the liposomes is a strategy with the potential of improving drug delivery and decrease systemic toxicity in pediatric population [22]. Next to antibodies and their fragments, peptides represent a versatile tool for targeted approaches due to the ease of synthetic production, conjugation, and stability under physiological conditions [23]. We identified by *in vivo* phage display novel peptides selectively binding to RMS cells [24,25]. One of the candidate-lead peptides, the furin-binding peptide TmR, was tested on RMS cells. Despite increased binding *in vitro,* no increased accumulation of VCR in RMS tumor compared to non-targeted VCR-loaded liposomes was observed *in vivo* [21]. Therefore, we used another approach and tested a panel of known tumor targeting peptides against RMS-overexpressed surface molecules [26]. The nucleolin (NUCL) targeting peptide F3, identified originally as the minimal sequence required for tumor homing of a fragment of HMGB1 isolated by *in vivo* phage display on tumor vasculature [27], was the best RMS-targeting peptide, with a stronger binding to RMS cells compared to TmR [26]. NUCL was subsequently identified as target of the F3 peptide by co-precipitation [28]. NUCL is a multifunctional protein localized primarily in the nucleolus, but also found in the nucleoplasm, cytoplasm, and cell membrane [29,30]. It is involved in several aspects of DNA metabolism, and participates extensively in RNA regulatory mechanisms [31]. NUCL overexpression and increased localization on the cell membrane of cancer cells and angiogenic blood vessels is a common feature of several cancers [28,32], making it an attractive target for cancer therapies [33–35]. Interestingly, recent pre-clinical studies have shown that pH-sensitive F3-modified liposomes loaded with doxorubicin are effective in targeting and suppressing tumor growth of mesothelioma [36], and of neuroblastoma tumors [37].

Here, we establish a rapid and robust microfluidic-based formulation of VCR-loaded liposomes functionalized with the NUCL-targeting F3 peptide. We have studied how F3-surface modification affects the drug loading and retention, and verified *in vitro* binding, internalization, and cytotoxicity of VCR-loaded liposomes in RMS cells.

2. Materials and methods

2.1. Materials

Egg sphingomyelin was provided by Lipoid (581010-2200003-01/901, Lipoid GmbH, Germany). Cholesterol (C3045) was purchased from Sigma Aldrich (Buchs, Switzerland). N-palmitoyl-sphingosine-1-{succinyl[methoxy(polyethylene glycol)2000]} (Avanti C16 PEG2000 Ceramide, 880180P), 1,2-distearoyl-*sn*-glycero-3-phosphoethanolamine-N-[maleimide(polyethylene glycol)-2000] ammonium salt (Avanti DSPE-PEG2000-maleimide, 880126P) were purchased from MERCK (Buchs, Switzerland). 1,1-dioctadecyl-3,3,3,3-tetramethylindotricarbocyanine iodide (DiO) was purchased from Abcam (ab189809). As control peptide, the AA peptide (ASKKPAANIKA) was chosen since it does not bind RMS cells as described previously [26]. F3 peptide (KDEPQRRSARLSAKPAPPKPEPKPKKAPAKK) and AA were modified with additional Cys at the C-terminus, with N-terminus acetylation and C-terminus amidation, and custom synthesized by Genecust at > 95 % purity (Boynes, France). 4′,6-Diamidino-2-phenyl-indol-dihydrochlorid (DAPI, D9542) and thiazolyl blue tetrazolium bromide (MTT, M2128) were purchased from Sigma Aldrich. Clinical grade Vincristine sulphate was purchased from Teva (Jona, Switzerland), and Doxorubicin (Adriblastin) from Pfizer (Zurich, Switzerland).

2.2. Cell lines

The rhabdomyosarcoma (RMS) cell lines RMS, Rh28, Rh30, Rh4, Rh5, JR and Rh36, Rh18, TTC-442, RUCH-3, RD, and human fetal lung fibroblast MRC-5 cells, kindly provided by Prof. Beat Schäfer (University Children's Hospital of Zurich), were cultivated in Dulbecco's modified Eagle's medium (1-26F01-I, BioConcept) with 10 % FBS (10270106, Thermo Fisher Scientific) and 100 U/mL penicillin, 100 μg/mL streptomycin (4-01F00-H, BioConcept). Immortalized human healthy primary myoblasts KM155C25Dist (referred to as myoblasts), kindly provided by the platform for immortalization of human cells MyoLine from the Institut de Myologie (Sorbonne University, Paris, France), were cultured in Skeletal Muscle Cell Growth Medium (C-23060, PromoCell), supplemented with Skeletal Muscle Cell Growth Medium SupplementMix (C-39365, PromoCell). RMS cells were verified by STR analysis and tested negative for mycoplasma.

2.3. Surface proteomics

Subconfluent cells from six P15 cell culture dishes (639160, Greiner Bio-One) were collected, and membrane/surface proteins were enriched by differential centrifugation as described previously [38]. Briefly, the plasma membrane protein fraction was enriched after removal of nuclei and other subcellular compartments and separated by SDS-PAGE. The enriched plasma membrane proteins were digested, loaded onto a precolumn (C18 PepMap 100, 5 μm, 100 A, 300 μm i.d. × 5 mm length, Thermo Fisher Scientific), and eluted in backflush mode onto a C18 column (CSH Waters column, 1.7 μm, 130 Å, 75 μm × 20 cm, Waters). The HPLC column effluent was directly coupled to a mass spectrometer via a nano-spray ESI source. The MaxQuant label-free quantification (LFQ) algorithm was used to analyze abundance of the peptides in the samples. LFQ (label-free quantitation) intensity was taken for quantification and ANOVA analysis of differential expression.

2.4. Conjugation reaction

The targeted liposomes were prepared by incorporating DSPE-PEG-peptide into the lipid layer of liposomes by performing pre-formulation conjugation of DSPE-PEG-maleimide with the C-terminal Cys (C) included in the peptides. In order to identify the most suitable and efficient solvent for the reaction, different conditions were tested (Supplementary Figure S1). Eventually, the peptide and DSPE-PEG-maleimide were mixed at a ratio 1:1, at a concentration of 1.2 mM, in anhydrous DMSO and stirred for 24 h at 25 °C.

Quantitative control was performed by taking aliquots of the reaction mixture for HPLC quantification of unreacted peptide as described below, in 2.10; qualitative control was performed by matrix-assisted laser desorption/ionization time-of-flight (MALDI-TOF). In details, an α-cyano-4-hydroxycinnamic acid matrix was used and mixed with an aliquot of reaction mixture prior to measurement. The yield of the conjugation reaction was defined by the following formula:

$$Conjugation\ efficiency\ (\%) = 100\% \times \frac{[Pept.\ initial] - [Pept.\ unreacted]}{[Pept.\ initial]}$$

2.5. Liposome formulation

Liposomes were formulated with egg sphingomyelin (E), cholesterol (C), PEG Ceramide (PEGC), DiO, and DSPE-PEG2000-maleimide (DPEG-mal) or DSPE-PEG2000-peptide (DPEG-pep) at the mol% ratio E:C:PEGC:DiO:DPEG-mal/DPEG-pep of 49.8:45:4:0.2:1 by microfluidic rapid mixing using the Nanoassemblr Ignite (Precision NanoSystems, Vancouver, Canada). The presence of DPEG-pep in the crude reaction was verified by MALDI. DPEG-pep conjugate was mixed with the lipid composition without any purification step due to high efficacy of the conjugation. Briefly, a 1 or 2 mL syringe containing the lipid mixture in ethanol:DMSO (58:42 v/v) was inserted in one of the two inlets. The second inlet had a 5 mL syringe with freshly filtered citrate buffer pH 3.0. Total concentration of the lipid solution prior to mixing was 33.27 mg/mL (50 mM). The microfluidics system was set up with a Total Flow Rate (TFR) of 12 mL/min; and a Flow Rate Ratio (FRR) of 3:1 of citrate buffer:EtOH. Initially, different FRRs, between 1.5:1 and 4.5:1, were tested. Ethanol was removed by dialysis against citrate buffer pH 3.0 using a Slide-A-Lyzer Dialysis Cassette G2 (87730, Thermo Fisher Scientific) for 2 h at 25 °C followed by buffer change and overnight dialysis at 4 °C. Ultrafiltration was performed with Amicon Ultra 0.4, 10 kDa MWCO (UFC801024, Merck Millipore) in order to concentrate the liposomes solutions. The concentration of the liposomes throughout the downstream procedures was quantified and equilibrated by measuring the fluorescence of DiO, to compensate possible losses after dialysis, ultrafiltration, and during drug loading. The concentration of liposomal formulations was indirectly monitored by measuring the fluorescence with a SpectraMax M2 microplate Reader (Molecular Devices, Bucher Biotech, Basel, Switzerland) with Excitation at 488 nm and Emission at 501 nm. For fluorescence-based experiments, the samples were normalized by DiO fluorescence assuming homogeneous incorporation.

Hydrodynamic diameter and polydispersity index (PDI) were measured by dynamic light scattering (DLS, Litesizer 500, Anton Paar, Buchs, Switzerland) before and after drug loading using refractive index of 1.46 and a viscosity of 0.8914 mPa/s in 10 mM NaCl at a total lipid concentration of approximately 0.5 mM in standard disposable polystyrene cuvettes (30 runs, 10 sec). Zeta potential of liposomes was measured via electrophoretic light scattering (ELS) according to Smoluchowski approximation with a Debye factor 1.5 (100 runs). Measurements were done in 10 mM NaCl using Omega Cuvette (Anton Paar).

2.6. Vincristine loading and liposomes stability

Vincristine sulfate (VCR) was remotely loaded into the liposomes by means of a transmembrane pH-gradient, as previously described [21]. Briefly, VCR solution was brought to pH 7.2 with 0.5 M Na_2HPO_4. First, liposomes buffer was changed from citrate buffer pH 3.0 to HBS buffer pH 7.4 (HEPES buffer saline: 20 mM HEPES, 150 mM NaCl) using Sephadex G25 column (PD MiniTrap, Sigma). A drug-to-lipid ratio of 0.1:1 w/w was chosen as the most effective for VCR encapsulation, and a mixture of liposomes with approximately 0.4 mg/mL VCR was incubated in a water bath at 65 °C for 1 h. Free VCR was removed by two subsequent ultrafiltration runs (UFC510024, Amicon Ultra 0.5, 100 kDa MWCO, Merck Millipore). The filtrate was recovered from the Ultracel® ultra-low protein binding regenerated cellulose membrane. The encapsulation efficiency (EE) was quantified according to the following equation: EE (%) = [VCR encapsulated]/[VCR total], where [VCR encapsulated] corresponds to the encapsulated VCR concentration determined by HPLC as described below in 2.10 and [VCR total] corresponds to the total VCR concentration. To test drug retention under physiological conditions, VCR-loaded liposomes were mixed with 50 % FBS in HBS pH 7.4 and incubated at 37 °C in a water bath. Initial concentration of VCR in liposomes was 40 μg/mL, with total lipid concentration of 0.4 mg/mL. Aliquots of 100 μL were taken after 0, 4, 8, 12, 24 and 48 h. The released VCR was separated from the liposomal VCR by ultracentrifugation (Optima™ MAX-XP centrifuge, Beckman Coulter, Nyon, Switzerland) at 100′000 x g for 3 h at 10 °C [39]. VCR in the supernatant was quantified by HPLC (see 2.10).

2.7. Flow cytometry

In vitro binding of liposomes to RMS cells was evaluated using flow cytometer CytoFLEX (Beckman Coulter). To achieve the optimal density of cells, 20′000 RD and Rh30 cells, 30′000 Rh4 cells, or 10′000 MRC-5 cells were plated in a 96-well plate and incubated overnight. Liposomes were added at a total lipid concentration of 0.01 mM in full growth medium for 2 h incubation at 37 °C and 5 % CO_2. Cells were washed twice with DPBS (D1408, Sigma Aldrich) and detached with Accutase for 10 min at 37 °C (Thermo Fisher Scientific). Gating strategy included debris and doublets discrimination as well as nonviable cells exclusion using 7-amino-actinomycin D (7-AAD, 00–6993-50, Thermo Fisher Scientific). The geometric mean of the fluorescent intensity (MFI) measured at 488 nm was used to quantify binding of liposomes formulated with the green lipophilic dye DiO. Data was analyzed with FlowJo v10.8 software (BD Life Sciences).

2.8. Fluorescence microscopy

To have the optimal cell confluency for internalization analysis by microscopy, 10′000 cells (Rh30, RD) or 20′000 (Rh4) were seeded on 8-well chamber cover glass slides (80826, Ibidi, Grafelfing, Germany). 17′500 cells (MRC-5) were seeded on 8-well chamber slide with removable wells (Nunc™ Lab-Tek™ II, 154534, Thermo Scientific). Cells were incubated with 0.5 mM liposomes (total lipid concentration) in full growth medium for 2 h at 37 °C in a humidified incubator with a 5 % CO_2 atmosphere. After incubation, cells were washed with 200 μL PBS, fixed with 2 % PFA (28908, Thermo Fisher Scientific) for 15 min at 25 °C. To remove residual fixator, cells were washed for 5 min three times with Tris saline buffer (TBS) and DAPI in TBS was added for 2 min prior to mounting with a chamber-compatible medium (50001, Ibidi). The confocal microscope LSM 710 (Carl Zeiss, Germany) was used to acquire and analyze Z-stacks by detecting DiO embedded in the liposome bilayer in RD, Rh4, and Rh30 cells (Ex/Em 485/500). The widefield microscope Axio Imager Z2 (Carl Zeiss, Feldbach, Switzerland) was used to acquire images of MRC-5 cells with a 40x objective. The images were further processed by ZEN 3.4 (blue edition) Software (Carl Zeiss).

2.9. MTT cell viability assay

Cytotoxicity of liposomes containing VCR was evaluated in RMS cell lines Rh30, Rh4, and RD. To achieve optimal cell density at the time of experiment, cells were seeded at a density per well of 2′500 cells for RD and Rh30, or 7′000 cells for MRC-5 in 96-well plates, grown overnight, and incubated in full growth medium with increasing concentrations of free VCR or liposomal encapsulated VCR for 2 h at 37 °C in a humidified incubator with a 5 % CO_2 atmosphere, followed by a wash with room-temperature PBS and growth medium replacement. Cells were incubated for additional 48 h and cell viability was analyzed according to standard MTT protocol. Briefly, 50 μL of MTT 5 mg/mL in PBS were added to the wells and incubated for 3.5 h at 37 °C, medium was removed and 150 μL MTT solvent (4 mM HCl, 0.1 % Nonidet P-40 (NP40) in isopropanol) were added. After 1 h RT under gentle shaking, the optical density (OD) was read at 590 nm with reference filter at 620 nm in a Sunrise spectrophotometer (Tecan). In order to define EC_{50}, the dose–response curve was plotted on the normalized values, where untreated cells were taken as 100 % and the bottom of the curve as 0 %. Normalized dose–response curves were fitted to the data points by nonlinear regression analysis using GraphPad Prism.

2.10. Clustering of surface nucleolin in the presence of micelles composed of F3 peptide

The experiment method was adapted from Fonseca et. al [36] as follows: 100′000 RD cells were incubated with 10 μg/mL anti-NCL-Alexa®488 antibody (mouse, 364–5 clone, Abcam) for 30 min at 37 °C in the presence or absence of 16.7 μM of LIPO-F3 or LIPO-AA in PBS with 1 % BSA. As controls, the respective IgG isotype was used at the same concentrations. Cells were then washed twice with PBS and stained nonviable cells exclusion using 7-amino-actinomycin D (7-AAD, 00–6993-50, Thermo Fisher Scientific). Liposomes were formulated as described above, but without the fluorescent dye DiO.

2.11. HPLC quantification of peptides and vincristine

The HPLC protocol to quantify unreacted peptides was developed using acetonitrile with 0.1 % trifluoroacetic acid (TFA) as mobile phase A and MilliQ water with 0.1 % TFA as mobile phase B. A linear gradient from 90 % B to 75 % was kept for 15 min, followed by 2 min with 75 % to 90 % B at a flow rate of 1 mL/min, with a reverse phase C18 column (Nucleosil 100–5 C18, 720014.40, Macherey-Nagel) maintained at 25 °C. The absorbance detection wavelength was set at 220 nm at UPLC system (Ultimate 3000 HPLC with DAD-3000, Thermo Fisher Scientific,).

VCR quantification was performed using a RP-18 (5 μm, L x I.D. 25 cm x 4.6 mm) LiChrospher® 100 column (Merck Millipore). Isocratic elution created by 68 % of phosphate buffer pH 3.2 (33 mM dipotassium phosphate, 22 mM phosphatic acid) and 32 % of acetonitrile/UPW 90/10 (v/v). Prior to run, liposomes were disrupted by mixing with EtOH (1:2, v/v), vortexing for 10 min, and centrifugation to remove any precipitate. Doxorubicin was added to a final concentration of 82 μg/mL and used as an internal standard. The length of the run was 16 min at a flow rate of 1.5 mL/min. The highest signal was measured at 296 nm.

2.12. Statistical analysis

Unless otherwise stated, statistical analysis was performed with GraphPad Prism software, version 10.1 (GraphPad Software, San Diego, CA). The statistical significance was evaluated by the paired Student's *t*-test and the Mann–Whitney test, with a threshold of $p < 0.05$.

3. Results

3.1. Nucleolin expression in rhabdomyosarcoma cell lines

As previously reported, quantum dots conjugated with the nucleolin (NUCL) binding peptide F3 bind very strongly to RMS cells but not to healthy cells [26]. Moreover, we showed that NUCL is overexpressed at the mRNA level in RMS patient samples compared to healthy muscle tissue [26]. High abundance of surface NUCL would support the use of NUCL-specific ligands for targeted therapy against RMS. However, no protein data was available about the presence of NUCL on the surface of RMS cells. Therefore, we have analyzed the data from a surfaceome analysis based on multi-step enrichment of membrane proteins by differential centrifugation with eleven RMS cell lines belonging to the two main RMS subtypes: alveolar, also called fusion positive (FP) (RMS, Rh5, Rh4, Rh30, Rh28, JR) and embryonal, also called fusion negative (FN) (Rh36, Rh18, TTC-442, RUCH-3 and RD) [38]. Healthy myoblasts, as well as embryonic fibroblasts (MRC-5) were used as negative control (Fig. 1).

NUCL expression levels were estimated by Label Free Quantification (LFQ). In nine RMS cell lines out of eleven, NUCL expression was significantly higher than in healthy myoblasts (Fig. 1a); and the fold change was at least 5-fold higher compared to myoblasts (Fig. 1b). These data confirm a significant abundance of NUCL on RMS cells compared to healthy cells and support the investigation of F3 peptide for RMS-specific active targeting.

3.2. DSPE-PEG-peptide synthesis

To create peptide-modified liposomes, we conjugated DPEG-mal to the F3 peptide by Michael addition reaction with the C-terminal Cysteine (C) of F3. As negative control for F3 peptide, we initially tested the scrambled peptide F3scrmbl (QPAPAPADKLKPKE-KEKSKSKRKRKRAPAVPPAP) described by Zhang et al. [40]. However, when conjugated to QD as described in [26], F3scrmbl showed a significant binding to RMS cells RD (Supplementary Figure S2). Therefore, we decided to use as a negative control the peptide NTP-AA (ASKK-PAANIKA), derived from the NCAM1 binding NTP peptide [41], which does not bind to RMS cells, as previously shown [26]. The control peptide NTP-AA (referred to as AA) with C-terminal Cysteine was conjugated with DPEG-mal.

To find the optimal conditions for efficient maleimide-cysteine conjugation not promoting peptide-dimer formation, we tested eighteen different combinations of solvents (Supplementary Table S1) and the reaction products were analyzed qualitatively by MALDI-TOF. In

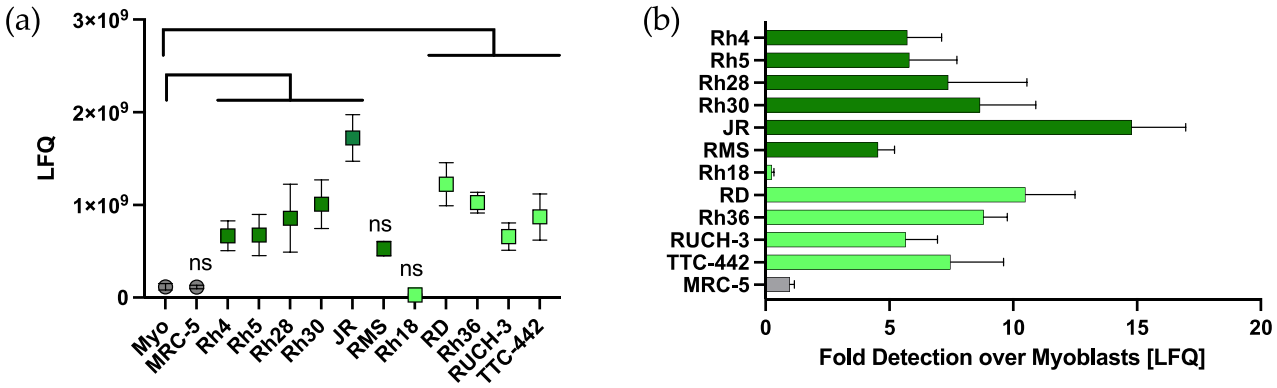

Fig. 1. Detection of cell surface NUCL by proteomics. Cells were harvested and cell membrane fraction was enriched by a two-step centrifugation process. Peptides from fragmented proteins were analyzed by LC-MS. (a) LFQ (label-free quantification) of NUCL protein intensity in the different RMS cell lines tested. Shown are mean values +/- S.D., n = 3. *$p < 0.02$ in one-way Anova test. ns: not significant (b) Fold change of NUCL label-free quantitation (LFQ) values compared to immortalized myoblasts (Myo). Dark green symbols indicate alveolar FP-RMS cell lines, whereas light green symbols indicate embryonal FN-RMS cell lines. Grey symbols indicate control cells. Shown are mean values +/- S.D., n = 3.

addition, since we aimed to create liposomes in a one-step microfluidic mixing, the selection of the reagents for the reaction was based also on the compatibility with the cartridge plastic. The best conditions for the conjugation reaction between DPEG-mal and the peptides C-terminal Cysteine were observed with DMSO (Supplementary Fig. S1). Via MALDI-TOF analysis, the typical peaks of DPEG-mal (MW ~ 2.9 kDa) could be detected (Fig. 2a). After 24 h incubation with DMSO at 25 °C, the DPEG-F3 conjugate with a MW of 6.5–6.6 kDa was detected (Fig. 2b). The unreacted peptides, with a peak visible in the mass spectrum at MW 3.5 kDa, were then quantified by HPLC. Both coupling reactions (DPEG-F3 and DPEG-AA) had an efficiency greater than 95 % (Fig. 2c).

3.3. Liposome formulation and vincristine encapsulation

In order to manufacture liposomes, a microfluidic mixer (Ignite®, Precision NanoSystems) was used and flow rate ratio (FRR) and total flow rate (TFR) were optimized for our lipid composition (E50:C45:PEGC4:DPEG-mal1). TFR of 12 mL/min and FRR of 3:1 were chosen (Supplementary Figure S3).

Three different formulations of PEGylated liposomes were created by microfluidic mixing: the non-conjugated liposomes, LIPO-NC, composed of E:C:PEGC:DiO:DPEG-mal; LIPO-AA, conjugated to the control peptide AA, composed of E:C:PEGC:DiO:DPEG-AA; and LIPO-F3 conjugated to the anti-NUCL peptide F3, composed of E:C:PEGC:DiO:DPEG-F3, as schematically represented in Fig. 3. The hydrodynamic diameter of the liposomes was measured by dynamic light scattering (DLS), and the particles were homogeneous (PDI < 0.18), with a mean size of 61.7–67.3 nm (Table 1).

VCR was remote-loaded into the liposomes by means of a transmembrane pH gradient. The encapsulation efficiency in non-conjugated liposomes (LIPO-NC) was around 92 %, higher than in peptide-modified liposomes, with 78.0 % for LIPO-AA and 69.5 % for LIPO-F3 (Fig. 4a). The mean size of the liposomes increased slightly after VCR-loading and was between 68.9 and 72.5 nm (Table 1, Fig. 4b).

3.4. Characterization and stability of liposome and VCR retention

Zeta potential was measured by electrophoretic light scattering (Fig. 4c). LIPO-NC had a mean zeta potential −0.28 mV, LIPO-AA had a slightly higher mean zeta-potential of +6.42, whereas LIPO-F3 had a mean zeta potential of +12.75 mV, significantly higher compared to

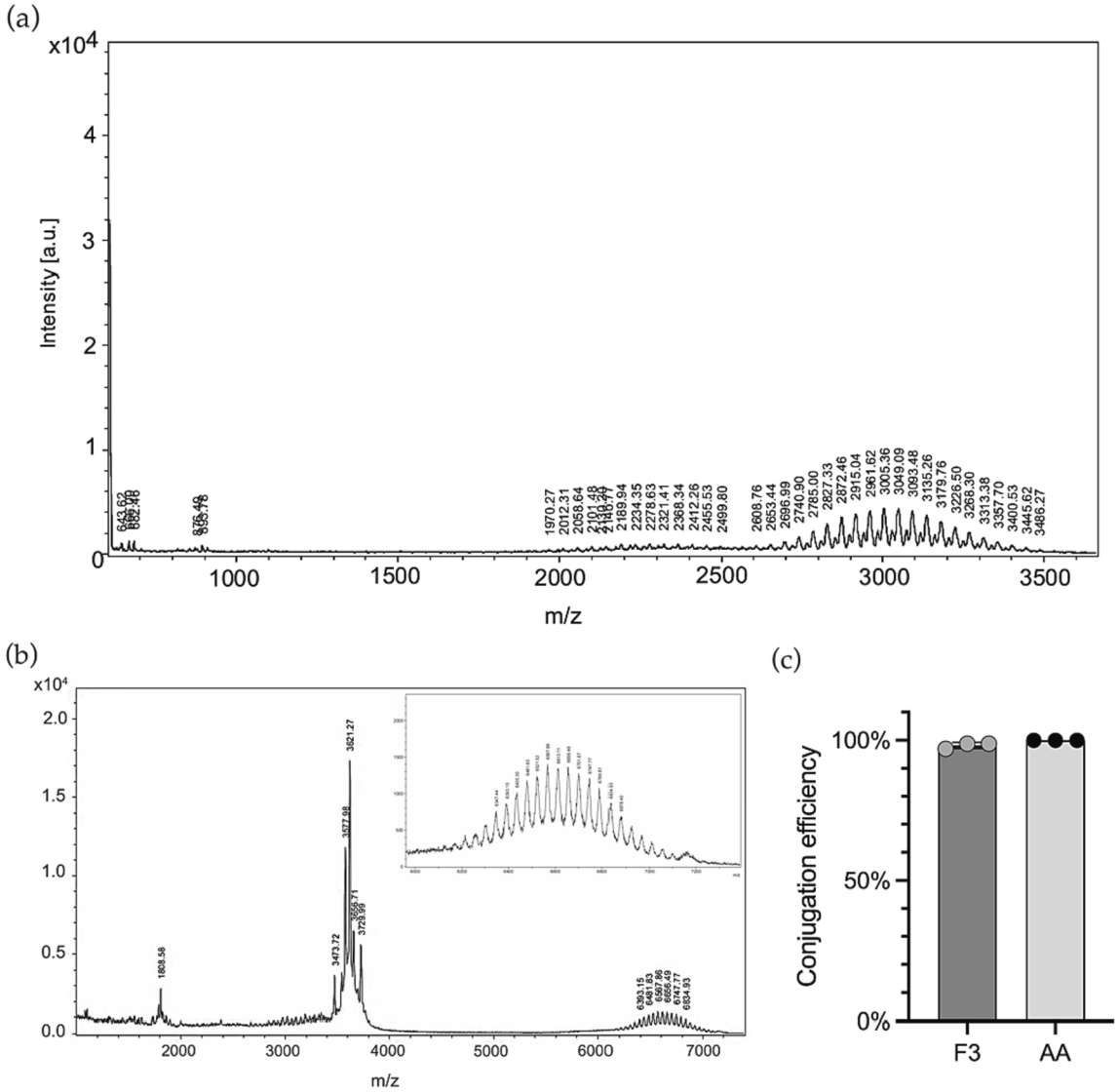

Fig. 2. DSPE-PEG-Maleimide conjugation to F3 peptide. (a) MALDI spectra of initial DPEG-mal (2.9–3 kDa) (b) MALDI spectra of the reaction mixture, DPEG-F3 (6.5–6.6 kDa), unreacted F3 peptide (3.577 kDa), unreacted DPEG-mal (2.9–3 kDa). (c) Conjugation efficiency of DPEG-mal to F3 peptide or to a control peptide AA, based on HPLC quantification of unreacted peptides, n = 3.

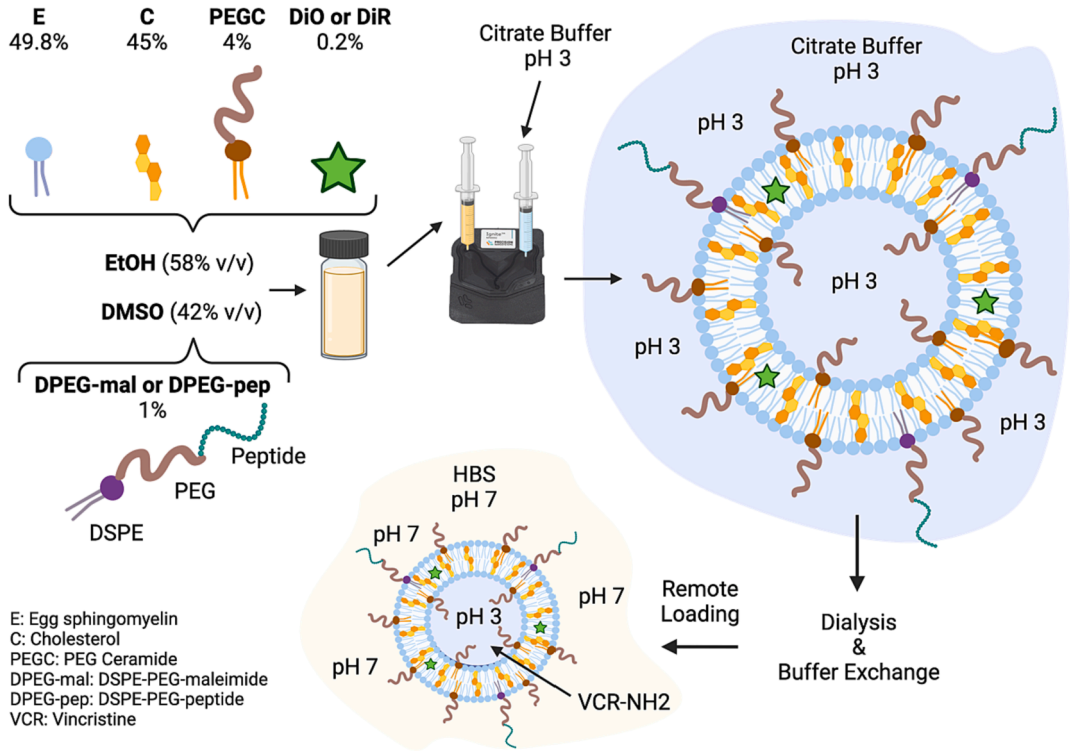

Fig. 3. Schematic representation of the liposome microfluidic formulation and remote loading of VCR driven by a pH-gradient. Lipids were mixed either in EtOH or in DMSO (DSPE-PEG-F3) and loaded to the first inlet (yellow) with organic phase. Citrate buffer pH 3.0 was loaded to the second inlet (light blue). Self-assembling liposomes were dialyzed against citrate buffer overnight. pH gradient allowed VCR in a neutral form to enter the liposomes and to be retained in a protonated form. Created with BioRender.

Table 1
Size and polydispersity index of liposomes before and after VCR encapsulation.

Liposome	Pre VCR encapsulation*		Post VCR encapsulation	
	Mean size [nm]	PDI, %	Mean size [nm]	PDI, %
LIPO-NC	66.7 ± 3.6	11.6 ± 7.3	72.5 ± 3.7	15.6 ± 4.7
LIPO-AA	67.3 ± 6.1	13.3 ± 9.1	71.4 ± 5.1	18.2 ± 4.2
LIPO-F3	61.7 ± 1.9	14.1 ± 4.8	68.9 ± 4.5	12.5 ± 3.3

* PDI and hydrodynamic diameter are presented as the mean ± SD (n ≥ 3 independent batches).

LIPO-NC and LIPO-AA. The zeta potential reflects surface charge of spherical nanoparticles, and in our liposomes it correlates with the presence of positively charged peptides. The net charge of the F3 peptide is 8 at pH 7.0 and the isoelectric point (pI) is 11.80. For AA peptide the net charge is 2.95 at pH 7.0 and the pI is 10.85. To determine the storage stability, the size of liposomes was measured after one month of storage in HBS Buffer at 4 °C and no change was observed indicating a good stability at these conditions (Fig. 4d, 4e).

To measure drug retention under physiological conditions, liposomes were incubated at 37 °C in 50 % FBS in HBS pH 7.4. The amount of released VCR was measured by HPLC in the supernatant after ultracentrifugation (Fig. 4f). After 24 h, LIPO-F3 released 35 % of encapsulated VCR, while LIPO-NC and LIPO-AA released about 50 % of the encapsulated drug. After 48 h an additional 10–20 % was released (Fig. 4f).

3.5. Liposomes binding to RMS cells and uptake

In order to evaluate the binding and uptake of peptide-modified liposomes by RD, Rh4, and Rh30 RMS cells, we used flow cytometry and confocal scanning microscopy. As control we included the human fetal lung fibroblast cell line MRC-5 that should express lower amount of NUCL (Fig. 1). After incubation of liposomes at 10 μM total lipid concentration with adherent cells for 2 h, the geometric mean fluorescence intensity (MFI) of the different samples was determined by flow cytometry, and the ratio to untreated cells was calculated as a proxy for liposomes binding to cells. LIPO-NC fluorescence intensities were similar to those of the untreated cells, ranging from 1.2- to 1.8-fold over untreated cells. When incubated with the RD cell line, LIPO-F3 showed a 14.7-fold higher binding compared to LIPO-AA, and a 42.1-fold higher binding compared to LIPO-NC. The binding of LIPO-F3 to Rh4 and Rh30 cells was also stronger than LIPO-AA, exhibiting 12.7-fold and 12.5-fold binding, respectively. Moreover, LIPO-F3 binding to Rh4 and Rh30 was 25.5-fold and 20.4-fold stronger than LIPO-NC, respectively (Fig. 5a). In contrast, incubation with MRC-5 fibroblasts did not show a particularly strong binding of the different liposomal formulations. LIPO-F3 showed only a 2.3-fold stronger binding compared to LIPO-AA and a 2.4-fold stronger binding compared to LIPO-NC. The MFI of MRC-5 cells incubated with LIPO-NC and LIPO-AA was identical with the fluorescence of untreated MRC-5. Interestingly, more than 96 % of RD, Rh4, and Rh30 cells incubated with LIPO-F3 resulted positive for the dye DiO, while upon incubation with LIPO-AA 44 % RD cells, 31 % Rh30 cells, and only 1 % Rh4 cells were positive. Only 2.4 % MRC-5 cells incubated with LIPO-F3 were positive, and MRC-5 incubated with LIPO-AA were all negative. These results suggest that F3-modified liposomes bind preferentially to RMS cells and that the binding correlates with the degree of NUCL expression in the cells.

In addition, to visualize the internalization, we incubated RD, Rh4, Rh30, and MRC-5 cells with liposomes at a final total lipid concentration of 0.5 mM. When incubated for 2 h prior to washing, LIPO-AA were not detected intracellularly, whereas LIPO-F3 internalization was evident in all the cells of the RMS cell lines within 2 h (Fig. 5b). In contrast, internalization of LIPO-F3 was visible only in few MRC-5 cells. These results show that only LIPO-F3 is rapidly internalized into RMS cells, in contrast to LIPO-AA, and further support the specificity of F3 for RMS

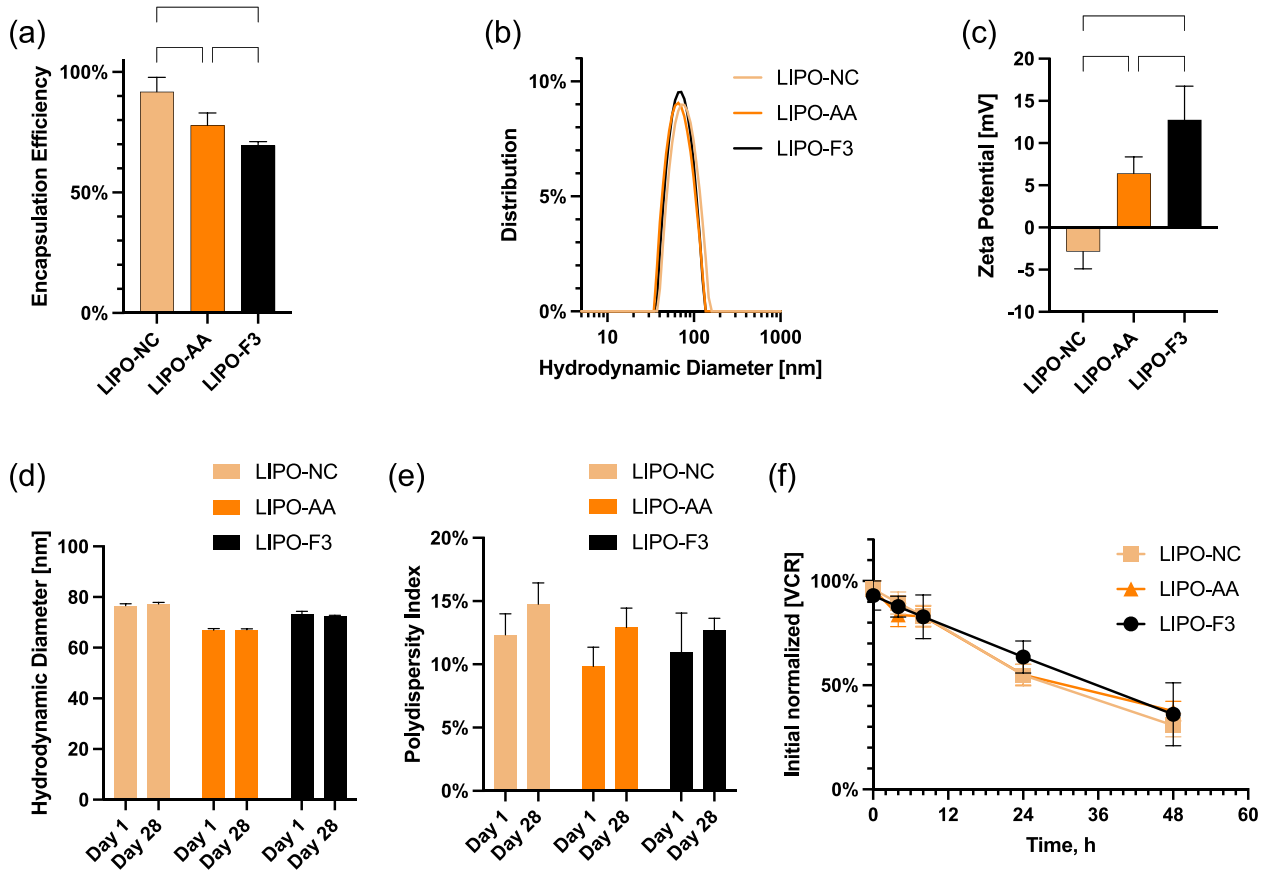

Fig. 4. Liposome characteristics. (a) Encapsulation efficiency of vincristine in the different liposomal formulation; not modified liposomes (LIPO-NC), control liposomes conjugated to unspecific peptide (LIPO-AA) and targeted liposomes (LIPO-F3). Data is presented as mean ± S.D (n = 3, three independent batches), **p < 0.01, ****p < 0.0001. (b) Size distribution of three different liposome formulations after VCR loading; control liposomes (LIPO-NC), conjugated to a control peptide (LIPO-AA), and F3 targeted liposomes (LIPO-F3). (c) Zeta potential of liposomes. n = 3, ****p < 0.0001. (d) Stability of liposomes after one month of storage at 4 °C determined by size and (e) polydispersity index. Stability experiments were performed on a single batch in triplicates. (f) VCR retention in the liposomes in a physiological buffer. Liposomes were incubated in 50 % FBS in HBS at 37 °C and aliquots were taken to separate free drug and liposomes by ultracentrifugation at 100′000 x g for 3 h at 10 °C. VCR was quantified by HPLC. Results from two independent batches are shown as mean ± S.D.

cells.

3.6. F3-mediated NUCL clustering

NUCL is primarily localized in the nucleus, but it can shuttle to the cell membrane [31]. NUCL does not have a transmembrane domain and is exposed to the extracellular side of the cell membrane in a complex with other proteins [32]. Several natural and synthetic anti-NUCL ligands bind to different extracellular portions of the protein. Detection of surface NUCL by FACS with anti-NUCL antibodies results however only in modest fluorescence intensity shifts as shown in multiple studies [28,42–44]. To further prove and quantify the presence of NUCL on the surface of RMS cells, we took advantage of the F3-stimulated clustering of NUCL on the cell surface. DSPE-PEG-F3 micelles were shown to stimulate the NUCL surface clustering and to increase remarkably detection by anti-NUCL antibodies [36]. We selected RD cells for these experiments, since they displayed a better binding by LIPO-F3 compared to Rh4 and Rh30 (Fig. 5a). When incubated with LIPO-F3 prior to staining with anti-NUCL antibodies, surface presence of NUCL on RD cells, as quantified by flow cytometry, increased from 16.1 % to 91.6 % (Fig. 6). Incubation with the negative control LIPO-AA increased the intensity of NUCL staining only up to 28.3 %. Thus, pre-treatment with LIPO-F3 leads to a 3.2-fold increase in detection of surface NUCL compared to LIPO-AA. The significant shift in NUCL detection only in the presence of F3-functionalized liposomes supports the specificity of F3 binding to NUCL.

3.7. In vitro cytotoxicity

The EC_{50} for RMS cells of non-encapsulated VCR and of VCR encapsulated in LIPO-NC, LIPO-AA, and LIPO-F3 was evaluated by MTT assay. The cells were incubated for 2 h with free VCR or liposomal VCR at varying drug concentrations from 1.37 nM to 9 μM (3-fold dilutions). Subsequently, the cells were washed to remove liposomes, in order to evaluate toxicity of bound liposomes and avoiding VCR release from unbound liposomes. Cells were cultured for additional 48 h with fresh medium (Fig. 7). The EC_{50} of VCR-LIPO-F3 for RD cells was 3.4 nM, similar to the EC_{50} of free VCR (2.87 nM), and 8.9- and 7.2-fold lower than VCR-LIPO-AA and VCR-LIPO-NC, respectively (Fig. 7a). For Rh30 cells, the EC_{50} of VCR-LIPO-F3 was 2.9 nM, 3-fold higher than the EC_{50} for free VCR (0.9 nM), but 2.7- and 3.4-fold lower than for control liposomes LIPO-AA and LIPO-NC, respectively (Fig. 7b). The EC_{50} of free VCR for MRC-5 was 27.8 nM, which is in range with the 90 nM IC50 reported in the literature [45]. The EC_{50} of VCR-LIPO-F3 for MRC-5 was 86 nM, 3-fold higher than the EC_{50} for free VCR, but 3.3- and 4.5-fold lower than for VCR-LIPO-AA and VCR-LIPO-NC, respectively. These results suggest an enhanced cytotoxic effect of VCR-LIPO-F3 formulation in RMS cells. Free VCR had an EC_{50} similar to VCR-LIPO-F3 in RD cells, 3-fold lower in Rh30 cells and MRC-5 cells.

In order to test the carrier effect of the different liposomal formulations, RMS cells and control fibroblasts MRC-5 were incubated with empty liposomes, not loaded with VCR, at the highest total lipid concentration used in the cytotoxic assays. The different liposomal

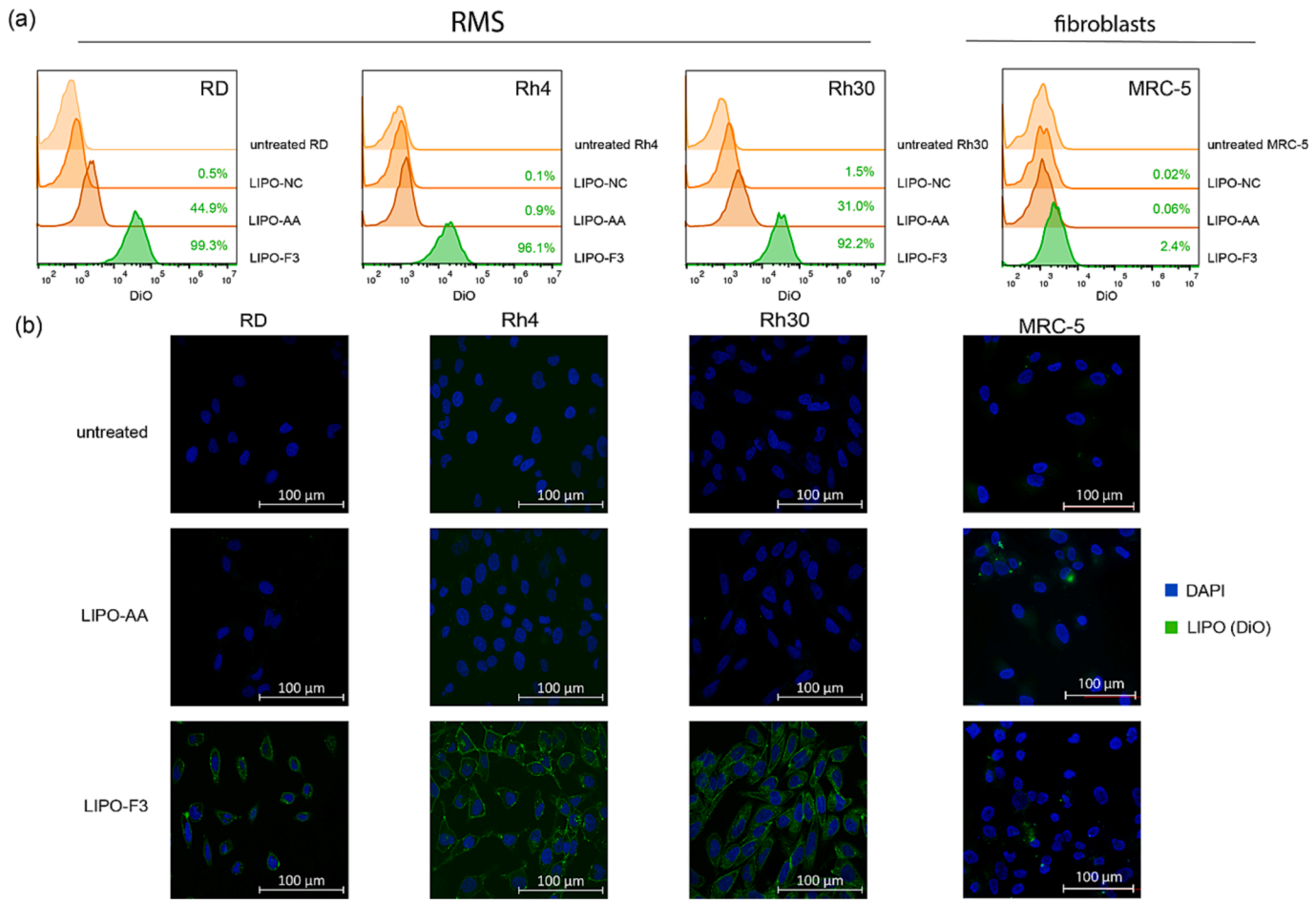

Fig. 5. Liposomes binding and internalization in RMS cells (a) Flow cytometry analysis performed after incubation of adherent cells with 10 µM liposomes for 2 h at 37 °C. This analysis was performed in at least three independent experiments, one representative experiment is shown. (b) Confocal microscopy shows internalization of DiO-labelled liposomes (green) in RMS cells after 2 h of incubation at concentration 0.5 mM (total lipid concentration). Normal fluorescence microscopy was performed with human fetal lung fibroblast cell line MRC-5. Cells were washed and fixed prior to analysis. Images shows overlay of nuclear staining with DAPI (blue) and DiO (green).

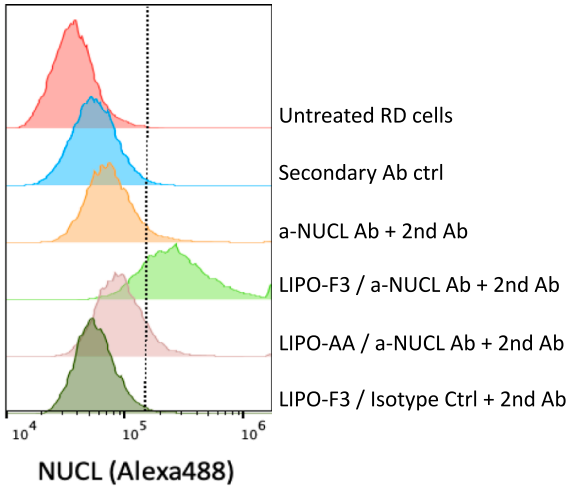

Fig. 6. Cell surface clustering of NUCL upon stimulation with LIPO-F3. Preincubation with LIPO-F3 increases cell surface presence of NUCL, allowing to detect the molecule by flow cytometry. RD cells were detached and incubated with liposomes for 30 min, washed twice and incubated with primary anti-NUCL antibodies (or isotype control). After incubation with secondary Alexa488-conjugated antibodies, the cells were washed and analyzed by FACS. This experiment was performed in duplicate.

formulations showed a modest effect on cell viability for RMS cells, inducing a decrease of 6 %–12 % for RD cells and 14 %–23 % for Rh30 cells. A stronger effect was visible in MRC-5 cells, with a decrease of up to 42 % for LIPO-AA. These data indicate that VCR-free liposomes are well tolerated by RMS cells and in this experimental setting contribute only marginally to their cytotoxicity. Human fibroblasts MRC-5 in contrast showed a stronger sensitivity to the incubation with VCR-free liposomes, which might also correlate with the fact that they are more delicate and sensitive to culture conditions. We conclude that LIPO-F3 bound to RMS cells and were internalized very efficiently within the 2 h timeframe to reach an EC_{50} similar or close to free VCR, a drug with high cell permeability [46].

4. Discussion

In this work, we developed a rapid, easily scalable, and robust microfluidic formulation of sphingomyelin/cholesterol-based PEGylated liposomes modified with the NUCL targeting peptide F3 and loaded with vincristine (VCR). After VCR encapsulation with efficiencies of up to 90 %, the liposomes had a favorable size of around 70 nm, were stable over one month at 4 °C, and retained the majority of encapsulated VCR after 24 h in serum at 37 °C. Size, PDI, stability, and VCR release from the liposomes was not affected by surface modification with peptides. F3-modified liposomes bound very efficiently to RMS cells and were internalized faster than control liposomes in RMS cell lines. *In vitro,*

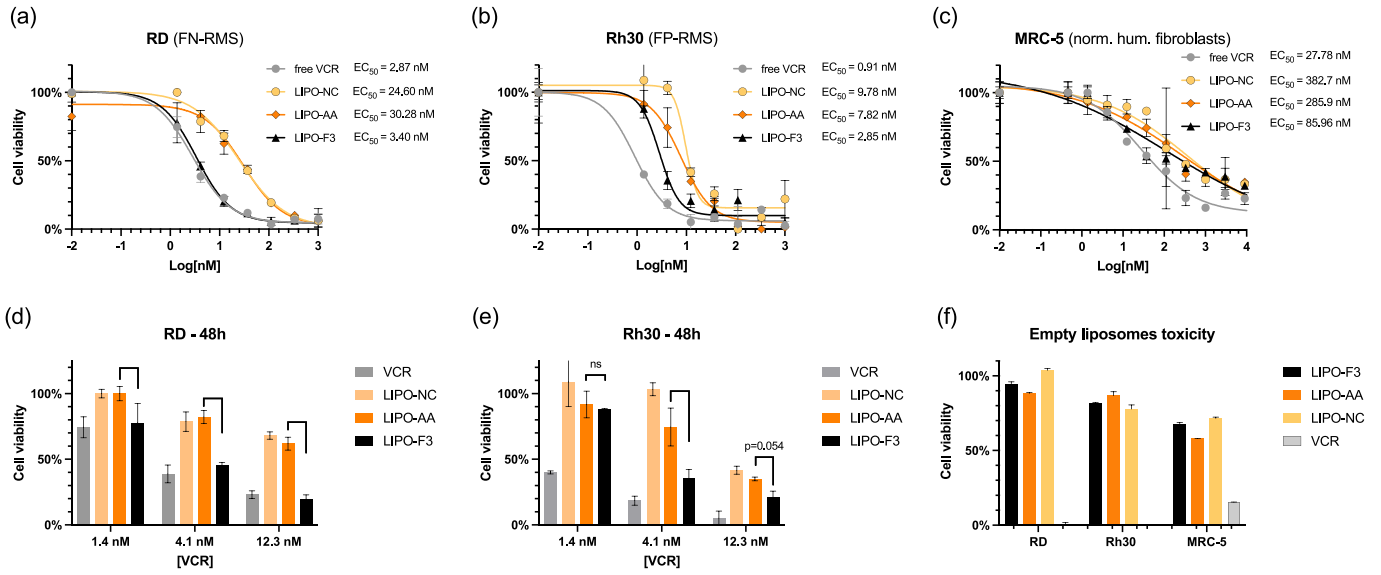

Fig. 7. Cytotoxicity of VCR and VCR-encapsulated liposomes against rhabdomyosarcoma cells. MTT assay was performed and EC_{50} determined after 2 h of treatment with 1.4 nM – 9 μM free VCR or equivalent liposomal VCR followed by 48 h incubation with fresh media of (a) RD cells, (b) Rh30, and (c) of human lung embryonal fibroblast cell line MRC-5, as control. (d, e) Viability of RMS cells after 48 h was analyzed for different concentrations of free VCR or liposomal VCR. n = 3 *p < 0.05, ** p < 0.01, ***p < 0.005. Statistical significance was verified by Mann-Witney test. (f) Carrier effect on cell viability of empty liposomes at the highest concentration used for the cytotoxic assays (9 μM). MTT assay was performed after 2 h of treatment with free VCR or empty liposomes followed by 48 h incubation with fresh media. Total lipid concentrations were: LIPO-NC: 2.3 mM, LIPO-AA: 1.8 mM, LIPO-F3: 2.2 mM. All experiments were conducted in triplicates.

VCR-loaded F3-liposomes decreased EC_{50} between 2- to 10-fold compared to control liposomes LIPO-NC an LIPO-AA.

While a certain adjustment of parameters has to be expected for different liposomal formulations, the rapidity and scalability are intrinsic to the microfluidics production method chosen [47–49]. It is important to specify that the scalability is not strictly dependent on the formulation used but rather on the employed manufacturing procedure. Indeed, with respect to the classical thin film formation and extrusion method to produce liposomes, a direct transfer of the critical process parameters from R&D development to commercial manufacturing is easier and a continuous flow microfluidic manufacturing allows to produce up to 48 L of particles per hour.

Marqibo®, a non-PEGylated sphingomyelin and cholesterol formulation of VCR, received accelerated FDA approval for the treatment of relapsed acute myeloid leukemia [50]. However, the FDA approval was withdrawn recently, due to the failure of a postmarking clinical trial to verify the clinical benefit of the drug attributed to the difficulties with patient recruitment [51].

Besides economical and strategical reasons, one additional reason behind this withdrawal might be found in the limited stability of Marqibo® [52]. PEGylation has a striking positive impact on circulation time and immune evasion of nanoparticles when administered intravenously and promotes long-term storage by preventing precipitation [21,52–55]. A more stable formulation might increase the clinical application of liposomal VCR. Moreover, passive tumor accumulation, is highly dependent on the different impact of the enhanced permeability and retention (EPR) effect [56], which is highly heterogeneous between pre-clinical models and human tumors, and within tumors [57–59]. Active targeting of nanoparticles to the tumor and its vasculature might obviate a possibly heterogeneous EPR effect in human tumors [12,60]. With this in mind, we developed a more stable, long circulating targeted version of Marqibo® [21]. The formulation included 4 % of PEG Ceramide (PEGC) and 1 % of DSPE-PEG2000 (DPEG) lipids and led to a prolonged circulation in the blood and increased accumulation of VCR in RMS tumors [21]. However, active targeting had no additional benefit. *In vitro,* liposomes targeted with the TmR peptide bound to RMS cells a modest 2-fold better than control peptide modified liposomes [21]. We hypothesized that a better binding was needed to further increase tumor accumulation *in vivo*. Hence, F3 peptide was identified as a better binder to RMS cells [26]. Here we report that F3-decorated liposomes bind to RMS cells at least 12-fold more compared to non-targeted control liposomes, a significant increase compared to TmR-liposomes.

The encapsulation efficiency of VCR by pH gradient was here slightly lower for peptide-modified liposomes (LIPO-AA and LIPO-F3) compared to non-conjugated liposomes (LIPO-NC). This could be due to the positive net charge of the peptides, *i.e.* the sum of the charges of the ionizable groups, which is 8 for peptide F3 and −2.95 for peptide AA. Negatively charged lipids such as DSPE-PEG are known to increase the membrane-water partition coefficient for positively charged drugs and improve their loading [61]. Conversely, a positive lipid might have the opposite effect. The zeta-potential data indicate a positive shift of surface charge.

In the present study, the modification of liposomes with peptide F3 did not impact the drug retention under physiological conditions as suggested by *in vitro* release experiment. In comparison to a non-PEGylated liposomal formulation with egg sphingomyelin/cholesterol 55/45, where 50 % drug retention was achieved after 5 h in 50 % FBS at 37 °C [62], our liposomes demonstrated longer drug retention of around 32–40 h at the same conditions. Here, VCR release for the three formulations was measured in the supernatant after liposomes centrifugation and was higher than the 10–20 % release we measured at 24 h with horizontal diffusion cells separated by a 200-nm pore size polycarbonate membrane [21]. However, it is within a range that should allow to achieve prolonged circulation in the bloodstream.

An important outcome of the present study is the validation of F3 peptide-mediated targeting of NUCL in RMS. NUCL is an abundant protein of the nucleus, highly expressed in exponentially growing cells [29], with multifaceted functions [32,63,64]. Its role in cancer has been extensively studied and discussed [32,65,66]. A number of ligands have been developed to target surface NUCL such as the pseudopeptides HB-19 [67], N6L [68], and the aptamer AS1411 [69,70], which have reached clinical trials for the treatment of various solid tumors (NCT01711398, NCT00740441). The first nanoparticles targeted with F3 peptide were PEGylated QDs used to deliver siRNA to knockdown EGFP expression in HeLa cells [71]. The first F3-modified pH-sensitive PEGylated liposomal formulation showed a very favorable

biodistribution of doxorubicin in a mouse breast cancer model, with preferential tumor accumulation [72]. In addition, the F3-modified pH sensitive liposomes have shown an extraordinary toxicity and pharmacokinetic profile in various pre-clinical animal models and therapeutic efficacy against mesothelioma [36].

We reported that F3-peptide is binding to RMS cells very strongly, and that NUCL mRNA expression levels are increased in RMS patient samples in comparison to healthy tissues [26]. NUCL was found to interact in RMS with the pro-oncogenic transcription factor TBX3 [73], and anti-NUCL oligonucleotide aptamers were shown to inhibit cell growth in embryonal RMS cells [74], suggesting a functional role in RMS progression. One limiting aspect of the study of cell surface NUCL by flow cytometry is the weak signal obtained with the available antibodies, probably also influenced by the active dynamics of NUCL transport. We were able to detect the enriched presence of NUCL on the surface of nine out of eleven RMS cell lines compared to healthy immortalized myoblasts and normal embryonic fibroblasts by antibody-independent surface proteomics. Moreover, by pre-treating RMS cells with F3-liposomes, thereby stimulating clustering of NUCL on the cell surface [36], we could observe a significant shift of the fluorescent signal detected by FACS supporting the specificity of the interaction between F3-liposomes and surface NUCL. These data support targeting of NUCL as relevant strategy also for RMS.

F3 peptide modification of liposomal VCR significantly increased delivery to RMS cells *in vitro*. Free VCR had an EC_{50} in the low nanomolar range (1–5 nM) which is in line with previous reports from other groups [45,75–78]. Here, we treated RMS cells and human embryonic fibroblasts MRC-5 cells as NUCL-low control, for 2 h before washing and changing the media to avoid the confounding effect of VCR released by unbound liposomes over 48 h. VCR-LIPO-F3 showed an EC_{50} significantly lower than VCR-LIPO-AA and the control liposomes VCR-LIPO-NC. Importantly, F3-liposomes showed a weaker binding to MRC-5 cells, which express less NUCL than RMS cells, as measured by FACS analysis and F3-liposomes loaded with VCR showed also a moderate toxicity against MRC-5 cells, supporting the specificity of F3-peptide for NUCL: These results are very promising and support future tests *in vivo*.

One limitation of this study is the lack of a proper negative control sequence for F3 peptide. In several studies, including the original work describing F3-NUCL interaction for the first time, an unrelated peptide with the sequence ARALPSQRSR was used as negative control [27,72]. In another study, a scrambled version of F3 peptide was used in two different forms, either conjugated to long PEG (3564 Da PEG, “exposed” scrambled), or short PEG (176 Da PEG, “buried” scrambled). Surprisingly, the “exposed” scrambled version on the surface of microbubbles still had 70 % of the binding capacity to the tumor vasculature compared to the exposed F3 [40]. Many randomly generated scrambled F3 sequences will contain positively charged clusters (K/R-enriched) potentially leading to unspecific interactions. Here, we chose the peptide NTP-AA (AA) as negative control since we knew it does not bind to RMS cells. NTP-AA is derived from the NCAM-1 binding peptide NTP, by substituting two Arginine (R) with two Alanine (A), eliminating the binding capacity to RMS cells [26].

5. Conclusions

In summary, the here reported NUCL targeting with F3-modified VCR-loaded liposomes provides a highly promising approach for targeted rhabdomyosarcoma treatment that might be used as an alternative to existing free VCR regimens with a better safety profile and possibly with a decreased dosing of the drug. The data provided here support the future investigation of the biodistribution profile and therapeutic efficacy of VCR-loaded F3-liposomes in preclinical RMS models.

Funding

This research was funded by the “Bernese Foundation for Children and Young Adults with Cancer / Berner Stiftung für krebskranke Kinder und Jugendliche”; by the Phospholipids Research Center, Heidelberg, Germany; Grant No. MBE-2020-079/2-1; and by the Mach-Gaensslen Foundation.

Institutional Review Board Statement: Not applicable.

Informed Consent Statement: Not applicable.

CRediT authorship contribution statement

Dzhangar Dzhumashev: Conceptualization, Methodology, Formal analysis, Data curation, Writing – original draft, Writing – review & editing, Visualization. **Stenija Anton-Joseph:** Methodology, Formal analysis, Writing – review & editing. **Victoria J. Morel:** Methodology, Writing – review & editing. **Andrea Timpanaro:** Methodology, Formal analysis, Writing – review & editing. **Gregor Bordon:** Methodology, Formal analysis. **Caroline Piccand:** Methodology, Writing – review & editing. **Simone Aleandri:** Methodology, Formal analysis, Writing – review & editing. **Paola Luciani:** Resources, Writing – review & editing. **Jochen Rössler:** Conceptualization, Writing – review & editing, Supervision, Project administration, Funding acquisition. **Michele Bernasconi:** Conceptualization, Methodology, Formal analysis, Data curation, Writing – original draft, Writing – review & editing, Visualization, Supervision, Project administration, Funding acquisition.

Declaration of Competing Interest

The authors declare that they have no known competing financial interests or personal relationships that could have appeared to influence the work reported in this paper.

Data availability

All the data generated in this paper are available upon reasonable request to M.B.

Acknowledgments

The authors would like to thank Dr. Despo Chatzikleanthous for the help and support with liposome formulation by microfluidic mixing; Sarah Teworte and Remo Eugster for their skilled help with HPLC analyses; and Dr. Anne Gregor for her kind assistance in fluorescent microscopy imaging. We acknowledge the staff of the Proteomics and Mass Spectrometry Core Facility (PMSCF), Department for BioMedical Research (DBMR), University of Bern for performing HPLC-MS and statistical analysis of surfaceome; as well as the Mass Spectrometry Service, Department of Chemistry, Biochemistry and Pharmaceutical Sciences (DCBP), University of Bern for MALDI-TOF analysis. We are also very grateful to Dr. Stephan Müller and the Flow Cytometryand Cell Sorting (FCCS) facility of the DBMR (University of Bern) for their support. We thank the Institute of Myology, Paris, France, for providing immortalized myoblasts.

Appendix A. Supplementary material

Supplementary Figure S1. MADLI-TOF spectra of conjugation reaction DSPE-PEG2000-Maleimide (2.9 kDa) with F3 peptide (3.577 kDa) under various conditions. Supplementary Figure S2. Binding of QD conjugated with F3 or F3scrmbl to RD cells. Supplementary Figure S3. Effect of the flow rate ratio (FRR) and the total flow rate (TFR) on E/C/PEGC/DPEG-mal liposomes’ hydrodynamic diameter and polydispersity index. Supplementary Figure S4. HPLC quantification of F3 peptide in conjugation reaction. Supplementary Table S1: Reaction conditions tested for the conjugation of DPEG-mal to peptides. References [79–94] are cited in the Supplementary Materials. Supplementary data to this article can be found online at https://doi.org/10.1016/j.ejpb.2023.11.020.

References

[1] M. Schindler, F.N. Belle, M.A. Grotzer, N.X. VonderWeid, C.E. Kuehni, Swiss Paediatric Oncology G., Childhood cancer survival in Switzerland (1976–2013): Time-trends and predictors, Int. J. Cancer 140 (2017) 62–74, https://doi.org/10.1002/ijc.30434.

[2] C.D.M. Fletcher, E.H. Baldini, J.Y. Blay, A. Gronchi, A.J. Lazar, C. Messiou, R. E. Pollock, S. Singer, in: WHO Classification of Tumours Soft Tissue and Bone Tumours, IARC Press, Lyon, 2020, pp. 201–215.

[3] F.G. Barr, L.M. Smith, J.C. Lynch, D. Strzelecki, D.M. Parham, S.J. Qualman, P. P. Breitfeld, Examination of gene fusion status in archival samples of alveolar rhabdomyosarcoma entered on the Intergroup Rhabdomyosarcoma Study-III trial: a report from the Children's Oncology Group, J. Mol. Diagn. 8 (2006) 202–208, https://doi.org/10.2353/jmoldx.2006.050124.

[4] D. Williamson, E. Missiaglia, A. de Reynies, G. Pierron, B. Thuille, G. Palenzuela, K. Thway, D. Orbach, M. Lae, P. Freneaux, et al., Fusion gene-negative alveolar rhabdomyosarcoma is clinically and molecularly indistinguishable from embryonal rhabdomyosarcoma, J. Clin. Oncol. 28 (2010) 2151–2158, https://doi.org/10.1200/JCO.2009.26.3814.

[5] S. Malempati, D.S. Hawkins, Rhabdomyosarcoma: review of the Children's Oncology Group (COG) Soft-Tissue Sarcoma Committee experience and rationale for current COG studies, Pediatr. Blood Cancer 59 (2012) 5–10, https://doi.org/10.1002/pbc.24118.

[6] C.B. Pratt, Response of childhood rhabdomyosarcoma to combination chemotherapy, J. Pediatr. 74 (1969) 791–794, https://doi.org/10.1016/s0022-3476(69)80145-9.

[7] D.S. Hawkins, Y.Y. Chi, J.R. Anderson, J. Tian, C.A.S. Arndt, L. Bomgaars, S. S. Donaldson, A. Hayes-Jordan, L. Mascarenhas, M.B. McCarville, et al., Addition of Vincristine and Irinotecan to Vincristine, Dactinomycin, and Cyclophosphamide Does Not Improve Outcome for Intermediate-Risk Rhabdomyosarcoma: A Report From the Children's Oncology Group, J. Clin. Oncol. 36 (2018) 2770–2777, https://doi.org/10.1200/JCO.2018.77.9694.

[8] G. Bisogno, G.L. De Salvo, C. Bergeron, S. Gallego Melcon, J.H. Merks, A. Kelsey, H. Martelli, V. Minard-Colin, D. Orbach, H. Glosli, et al., Vinorelbine and continuous low-dose cyclophosphamide as maintenance chemotherapy in patients with high-risk rhabdomyosarcoma (RMS 2005): a multicentre, open-label, randomised, phase 3 trial, Lancet Oncol. 20 (2019) 1566–1575, https://doi.org/10.1016/S1470-2045(19)30617-5.

[9] L. Tramsen, K. Bochennek, M. Sparber-Sauer, E. Salzmann-Manrique, M. Scheer, T. Dantonello, A. Borkhardt, U. Dirksen, A. Thorwarth, J. Greiner, et al., Pediatric Patients with Stage IV Rhabdomyosarcoma Significantly Benefit from Long-Term Maintenance Therapy: Results of the CWS-IV 2002 and the CWS DOK IV 2004-Trials, Cancers (Basel) (2023) 15, https://doi.org/10.3390/cancers15072050.

[10] M.E. van de Velde, M.H. van den Berg, G.J.L. Kaspers, F.C.H. Abbink, J.W.R. Twisk, I.M. van der Sluis, C. van den Bos, M.M. van den Heuvel-Eibrink, H. Segers, C. Chantrain, et al., The association between vincristine-induced peripheral neuropathy and health-related quality of life in children with cancer, Cancer Med. 10 (2021) 8172–8181, https://doi.org/10.1002/cam4.4289.

[11] S. Triarico, A. Romano, G. Attina, M.A. Capozza, P. Maurizi, S. Mastrangelo, A. Ruggiero, Vincristine-Induced Peripheral Neuropathy (VIPN) in Pediatric Tumors: Mechanisms, Risk Factors, Strategies of Prevention and Treatment, Int. J. Mol. Sci. 22 (2021), https://doi.org/10.3390/ijms22084112.

[12] S.N. Bhatia, X. Chen, M.A. Dobrovolskaia, T. Lammers, Cancer nanomedicine, Nat. Rev. Cancer 22 (2022) 550–556, https://doi.org/10.1038/s41568-022-00496-9.

[13] T.M. Allen, P.R. Cullis, Liposomal drug delivery systems: from concept to clinical applications, Adv. Drug Deliv. Rev. 65 (2013) 36–48, https://doi.org/10.1016/j.addr.2012.09.037.

[14] H.A. Yousefi Rizi, D. Hoon Shin, S. Yousefi Rizi, Polymeric Nanoparticles in Cancer Chemotherapy: A Narrative Review, Iran. J. Public Health 51 (2022) 226–239, https://doi.org/10.18502/ijph.v51i2.8677.

[15] S. Bayda, M. Hadla, S. Palazzolo, P. Riello, G. Corona, G. Toffoli, F. Rizzolio, Inorganic Nanoparticles for Cancer Therapy: A Transition from Lab to Clinic, Curr. Med. Chem. 25 (2018) 4269–4303, https://doi.org/10.2174/0929867325666171229141156.

[16] S. Yang, M. Wallach, A. Krishna, R. Kurmasheva, S. Sridhar, Recent Developments in Nanomedicine for Pediatric Cancer, J. Clin. Med. 10 (2021), https://doi.org/10.3390/jcm10071437.

[17] A. Gabizon, H. Shmeeda, Y. Barenholz, Pharmacokinetics of pegylated liposomal Doxorubicin: review of animal and human studies, Clin. Pharmacokinet. 42 (2003) 419–436, https://doi.org/10.2165/00003088-200342050-00002.

[18] C.E. Swenson, L.E. Bolcsak, G. Batist, T.H. Guthrie Jr., K.H. Tkaczuk, H. Boxenbaum, L. Welles, S.C. Chow, R. Bhamra, P. Chaikin, Pharmacokinetics of doxorubicin administered i.v. as Myocet (TLC D-99; liposome-encapsulated doxorubicin citrate) compared with conventional doxorubicin when given in combination with cyclophosphamide in patients with metastatic breast cancer, Anticancer Drugs 14 (2003) 239–246, https://doi.org/10.1097/00001813-200303000-00008.

[19] J.A. Silverman, S.R. Deitcher, Marqibo(R) (vincristine sulfate liposome injection) improves the pharmacokinetics and pharmacodynamics of vincristine, Cancer Chemother. Pharmacol. 71 (2013) 555–564, https://doi.org/10.1007/s00280-012-2042-4.

[20] N.N. Shah, M.S. Merchant, D.E. Cole, N. Jayaprakash, D. Bernstein, C. Delbrook, K. Richards, B.C. Widemann, A.S. Wayne, Vincristine Sulfate Liposomes Injection (VSLI, Marqibo(R)): Results From a Phase I Study in Children, Adolescents, and Young Adults With Refractory Solid Tumors or Leukemias, Pediatr. Blood Cancer 63 (2016) 997–1005, https://doi.org/10.1002/pbc.25937.

[21] M. Roveri, A. Pfohl, P. Jaaks, N. Alijaj, J.C. Leroux, P. Luciani, M. Bernasconi, Prolonged circulation and increased tumor accumulation of liposomal vincristine in a mouse model of rhabdomyosarcoma, Nanomedicine (Lond.) 12 (2017) 1135–1151, https://doi.org/10.2217/nnm-2017-0430.

[22] D. Rosenblum, N. Joshi, W. Tao, J.M. Karp, D. Peer, Progress and challenges towards targeted delivery of cancer therapeutics, Nat. Commun. 9 (2018) 1410, https://doi.org/10.1038/s41467-018-03705-y.

[23] M. Roveri, M. Bernasconi, J.C. Leroux, P. Luciani, Peptides for tumor-specific drug targeting: state of the art and beyond, J. Mater. Chem. B 5 (2017) 4348–4364, https://doi.org/10.1039/c7tb00318h.

[24] H. Witt, K. Hajdin, K. Iljin, O. Greiner, F.K. Niggli, B.W. Schafer, M. Bernasconi, Identification of a rhabdomyosarcoma targeting peptide by phage display with sequence similarities to the tumour lymphatic-homing peptide LyP-1, Int. J. Cancer 124 (2009) 2026–2032, https://doi.org/10.1002/ijc.24170.

[25] K. Hajdin, V. D'Alessandro, F.K. Niggli, B.W. Schafer, M. Bernasconi, Furin targeted drug delivery for treatment of rhabdomyosarcoma in a mouse model, PLoS One 5 (2010) e10445.

[26] D. Dzhumashev, A. Timpanaro, S. Ali, A.J. De Micheli, K. Mamchaoui, I. Cascone, J. Rossler, M. Bernasconi, Quantum Dot-Based Screening Identifies F3 Peptide and Reveals Cell Surface Nucleolin as a Therapeutic Target for Rhabdomyosarcoma, Cancers (Basel) (2022) 14, https://doi.org/10.3390/cancers14205048.

[27] K. Porkka, P. Laakkonen, J.A. Hoffman, M. Bernasconi, E. Ruoslahti, A fragment of the HMGN2 protein homes to the nuclei of tumor cells and tumor endothelial cells in vivo, PNAS 99 (2002) 7444–7449, https://doi.org/10.1073/pnas.062189599.

[28] S. Christian, J. Pilch, M.E. Akerman, K. Porkka, P. Laakkonen, E. Ruoslahti, Nucleolin expressed at the cell surface is a marker of endothelial cells in angiogenic blood vessels, J. Cell Biol. 163 (2003) 871–878, https://doi.org/10.1083/jcb.200304132.

[29] B. Lapeyre, H. Bourbon, F. Amalric, Nucleolin, the major nucleolar protein of growing eukaryotic cells: an unusual protein structure revealed by the nucleotide sequence, PNAS 84 (1987) 1472–1476, https://doi.org/10.1073/pnas.84.6.1472.

[30] J.S. Deng, B. Ballou, J.K. Hofmeister, Internalization of anti-nucleolin antibody into viable HEp-2 cells, Mol. Biol. Rep. 23 (1996) 191–195, https://doi.org/10.1007/BF00351168.

[31] K. Abdelmohsen, M. Gorospe, RNA-binding protein nucleolin in disease, RNA Biol. 9 (2012) 799–808, https://doi.org/10.4161/rna.19718.

[32] C.M. Berger, X. Gaume, P. Bouvet, The roles of nucleolin subcellular localization in cancer, Biochimie 113 (2015) 78–85, https://doi.org/10.1016/j.biochi.2015.03.023.

[33] M. Koutsioumpa, E. Papadimitriou, Cell surface nucleolin as a target for anti-cancer therapies, Recent Pat. Anticancer Drug Discov. 9 (2014) 137–152, https://doi.org/10.2174/1574892808666131119095953.

[34] S. Romano, N. Fonseca, S. Simoes, J. Goncalves, J.N. Moreira, Nucleolin-based targeting strategies for cancer therapy: from targeted drug delivery to cytotoxic ligands, Drug Discov. Today 24 (2019) 1985–2001, https://doi.org/10.1016/j.drudis.2019.06.018.

[35] B. Ferrara, S. Belbekhouche, D. Habert, C. Houppe, B. Vallee, S. Bourgoin-Voillard, J.L. Cohen, I. Cascone, J. Courty, Cell surface nucleolin as active bait for nanomedicine in cancer therapy: a promising option, Nanotechnology 32 (2021), https://doi.org/10.1088/1361-6528/abfb30.

[36] N.A. Fonseca, A.C. Gregório, V.M. Mendes, R. Lopes, T. Abreu, N. Gonçalves, B. Manadas, M. Lacerda, P. Figueiredo, M. Pereira, et al., GMP-grade nanoparticle targeted to nucleolin downregulates tumor molecular signature, blocking growth and invasion, at low systemic exposure, Nano Today 37 (2021), https://doi.org/10.1016/j.nantod.2021.101095.

[37] C. Brignole, V. Bensa, N.A. Fonseca, G. Del Zotto, S. Bruno, A.F. Cruz, F. Malaguti, B. Carlini, F. Morandi, E. Calarco, et al., Cell surface Nucleolin represents a novel cellular target for neuroblastoma therapy, J. Exp. Clin. Cancer Res. 40 (2021) 180, https://doi.org/10.1186/s13046-021-01993-9.

[38] A. Timpanaro, C. Piccand, A.C. Uldry, P.K. Bode, D. Dzhumashev, R. Sala, M. Heller, J. Rossler, M. Bernasconi, Surfaceome Profiling of Cell Lines and Patient-Derived Xenografts Confirm FGFR4, NCAM1, CD276, and Highlight AGRL2, JAM3, and L1CAM as Surface Targets for Rhabdomyosarcoma, Int. J. Mol. Sci. 24 (2023), https://doi.org/10.3390/ijms24032601.

[39] K. Nakamura, K. Yoshino, K. Yamashita, H. Kasukawa, Designing a novel in vitro drug-release-testing method for liposomes prepared by pH-gradient method, Int. J. Pharm. 430 (2012) 381–387, https://doi.org/10.1016/j.ijpharm.2012.04.011.

[40] H. Zhang, E.S. Ingham, M.K. Gagnon, L.M. Mahakian, J. Liu, J.L. Foiret, J. K. Willmann, K.W. Ferrara, In vitro characterization and in vivo ultrasound molecular imaging of nucleolin-targeted microbubbles, Biomaterials 118 (2017) 63–73, https://doi.org/10.1016/j.biomaterials.2016.11.026.

[41] L.C. Ronn, M. Olsen, S. Ostergaard, V. Kiselyov, V. Berezin, M.T. Mortensen, M. H. Lerche, P.H. Jensen, V. Soroka, J.L. Saffell, et al., Identification of a neuritogenic ligand of the neural cell adhesion molecule using a combinatorial library of synthetic peptides, Nat. Biotechnol. 17 (1999) 1000–1005, https://doi.org/10.1038/13697.

[42] T. Watanabe, K. Hirano, A. Takahashi, K. Yamaguchi, M. Beppu, H. Fujiki, M. Suganuma, Nucleolin on the cell surface as a new molecular target for gastric cancer treatment, Biol. Pharm. Bull. 33 (2010) 796–803, https://doi.org/10.1248/bpb.33.796.

[43] Y. Ding, N. Song, C. Liu, T. He, W. Zhuo, X. He, Y. Chen, X. Song, Y. Fu, Y. Luo, Heat shock cognate 70 regulates the translocation and angiogenic function of nucleolin, Arterioscler. Thromb. Vasc. Biol. 32 (2012) e126–e134, https://doi.org/10.1161/ATVBAHA.112.247502.

[44] S.C. Chen, T.H. Hu, C.C. Huang, M.L. Kung, T.H. Chu, L.N. Yi, S.T. Huang, H. H. Chan, J.H. Chuang, L.F. Liu, et al., Hepatoma-derived growth factor/nucleolin

axis as a novel oncogenic pathway in liver carcinogenesis, Oncotarget 6 (2015) 16253–16270, https://doi.org/10.18632/oncotarget.3608.
[45] Y. Mu, Y. Liu, L. Li, C. Tian, H. Zhou, Q. Zhang, B. Yan, The novel tubulin polymerization inhibitor MHPT exhibits selective anti-tumor activity against rhabdomyosarcoma in vitro and in vivo, PLoS One 10 (2015) e0121806.
[46] J. Pallares-Trujillo, C. Domenech, M.R. Grau-Oliete, M.P. Rivera-Fillat, Role of cell cholesterol in modulating vincristine uptake and resistance, Int. J. Cancer 55 (1993) 667–671, https://doi.org/10.1002/ijc.2910550426.
[47] C. Webb, N. Forbes, C.B. Roces, G. Anderluzzi, G. Lou, S. Abraham, L. Ingalls, K. Marshall, T.J. Leaver, J.A. Watts, et al., Using microfluidics for scalable manufacturing of nanomedicines from bench to GMP: A case study using protein-loaded liposomes, Int. J. Pharm. 582 (2020), 119266, https://doi.org/10.1016/j.ijpharm.2020.119266.
[48] C.B. Roces, E.C. Port, N.N. Daskalakis, J.A. Watts, J.W. Aylott, G.W. Halbert, Y. Perrie, Rapid scale-up and production of active-loaded PEGylated liposomes, Int. J. Pharm. 586 (2020), 119566, https://doi.org/10.1016/j.ijpharm.2020.119566.
[49] N. Forbes, M.T. Hussain, M.L. Briuglia, D.P. Edwards, J.H.T. Horst, N. Szita, Y. Perrie, Rapid and scale-independent microfluidic manufacture of liposomes entrapping protein incorporating in-line purification and at-line size monitoring, Int. J. Pharm. 556 (2019) 68–81, https://doi.org/10.1016/j.ijpharm.2018.11.060.
[50] Oncology (Williston Park) 26 (2012) 841.
[51] L.K. Roth, Acrotech Biopharma LLC; Withdrawal of Approval of New Drug Application for MARQIBO (VinCRIStine Sulfate LIPOSOME Injection), 5 milligrams/5 milliliters Federal Register 87 (2022) 25644-25645, https://www.regulations.gov/docket/FDA-2022-N-0354.
[52] W. Mao, F. Wu, R.J. Lee, W. Lu, J. Wang, Development of a stable single-vial liposomal formulation for vincristine, Int. J. Nanomed. 14 (2019) 4461–4474, https://doi.org/10.2147/IJN.S205276.
[53] M.S. Webb, D. Saxon, F.M. Wong, H.J. Lim, Z. Wang, M.B. Bally, L.S. Choi, P. R. Cullis, L.D. Mayer, Comparison of different hydrophobic anchors conjugated to poly(ethylene glycol): effects on the pharmacokinetics of liposomal vincristine, BBA 1372 (1998) 272–282, https://doi.org/10.1016/s0005-2736(98)00077-7.
[54] M.J. Johnston, S.C. Semple, S.K. Klimuk, S. Ansell, N. Maurer, P.R. Cullis, Characterization of the drug retention and pharmacokinetic properties of liposomal nanoparticles containing dihydrosphingomyelin, BBA 1768 (2007) 1121–1127, https://doi.org/10.1016/j.bbamem.2007.01.019.
[55] P. Milla, F. Dosio, L. Cattel, PEGylation of proteins and liposomes: a powerful and flexible strategy to improve the drug delivery, Curr. Drug Metab. 13 (2012) 105–119, https://doi.org/10.2174/138920012798356934.
[56] Y. Matsumura, H. Maeda, A new concept for macromolecular therapeutics in cancer chemotherapy: mechanism of tumoritropic accumulation of proteins and the antitumor agent smancs, Cancer Res. 46 (1986) 6387–6392.
[57] F. Danhier, To exploit the tumor microenvironment: Since the EPR effect fails in the clinic, what is the future of nanomedicine? J. Control. Release 244 (2016) 108–121, https://doi.org/10.1016/j.jconrel.2016.11.015.
[58] S.K. Golombek, J.N. May, B. Theek, L. Appold, N. Drude, F. Kiessling, T. Lammers, Tumor targeting via EPR: Strategies to enhance patient responses, Adv. Drug Deliv. Rev. 130 (2018) 17–38, https://doi.org/10.1016/j.addr.2018.07.007.
[59] M. Hashida, Advocation and advancements of EPR effect theory in drug delivery science: A commentary, J. Control. Release 346 (2022) 355–357, https://doi.org/10.1016/j.jconrel.2022.04.031.
[60] R. van der Meel, E. Sulheim, Y. Shi, F. Kiessling, W.J.M. Mulder, T. Lammers, Smart cancer nanomedicine, Nat. Nanotechnol. 14 (2019) 1007–1017, https://doi.org/10.1038/s41565-019-0567-y.
[61] E. Maurer-Spurej, K.F. Wong, N. Maurer, D.B. Fenske, P.R. Cullis, Factors influencing uptake and retention of amino-containing drugs in large unilamellar vesicles exhibiting transmembrane pH gradients, BBA 1416 (1999) 1–10, https://doi.org/10.1016/s0005-2736(98)00204-1.
[62] I.V. Zhigaltsev, N. Maurer, Q.F. Akhong, R. Leone, E. Leng, J. Wang, S.C. Semple, P. R. Cullis, Liposome-encapsulated vincristine, vinblastine and vinorelbine: a comparative study of drug loading and retention, J. Control. Release 104 (2005) 103–111, https://doi.org/10.1016/j.jconrel.2005.01.010.
[63] F. Mongelard, P. Bouvet, Nucleolin: a multiFACeTed protein, Trends Cell Biol. 17 (2007) 80–86, https://doi.org/10.1016/j.tcb.2006.11.010.
[64] H. Ginisty, H. Sicard, B. Roger, P. Bouvet, Structure and functions of nucleolin, J. Cell Sci. 112 (Pt 6) (1999) 761–772, https://doi.org/10.1242/jcs.112.6.761.
[65] H. Fujiki, T. Watanabe, M. Suganuma, Cell-surface nucleolin acts as a central mediator for carcinogenic, anti-carcinogenic, and disease-related ligands, J. Cancer Res. Clin. Oncol. 140 (2014) 689–699, https://doi.org/10.1007/s00432-014-1587-5.
[66] L.S. Carvalho, N. Goncalves, N.A. Fonseca, J.N. Moreira, Cancer Stem Cells and Nucleolin as Drivers of Carcinogenesis, Pharmaceuticals (Basel) 14 (2021), https://doi.org/10.3390/ph14010060.
[67] D. Destouches, D. El Khoury, Y. Hamma-Kourbali, B. Krust, P. Albanese, P. Katsoris, G. Guichard, J.P. Briand, J. Courty, A.G. Hovanessian, Suppression of tumor growth and angiogenesis by a specific antagonist of the cell-surface expressed nucleolin, PLoS One 3 (2008) e2518.
[68] D. Destouches, N. Page, Y. Hamma-Kourbali, V. Machi, O. Chaloin, S. Frechault, C. Birmpas, P. Katsoris, J. Beyrath, P. Albanese, et al., A simple approach to cancer therapy afforded by multivalent pseudopeptides that target cell-surface nucleoproteins, Cancer Res. 71 (2011) 3296–3305, https://doi.org/10.1158/0008-5472.CAN-10-3459.
[69] P.J. Bates, D.A. Laber, D.M. Miller, S.D. Thomas, J.O. Trent, Discovery and development of the G-rich oligonucleotide AS1411 as a novel treatment for cancer, Exp. Mol. Pathol. 86 (2009) 151–164, https://doi.org/10.1016/j.yexmp.2009.01.004.
[70] R. Yazdian-Robati, P. Bayat, F. Oroojalian, M. Zargari, M. Ramezani, S.M. Taghdisi, K. Abnous, Therapeutic applications of AS1411 aptamer, an update review, Int. J. Biol. Macromol. 155 (2020) 1420–1431, https://doi.org/10.1016/j.ijbiomac.2019.11.118.
[71] A.M. Derfus, A.A. Chen, D.H. Min, E. Ruoslahti, S.N. Bhatia, Targeted quantum dot conjugates for siRNA delivery, Bioconjug. Chem. 18 (2007) 1391–1396, https://doi.org/10.1021/bc060367e.
[72] V. Moura, M. Lacerda, P. Figueiredo, M.L. Corvo, M.E. Cruz, R. Soares, M.C. de Lima, S. Simoes, J.N. Moreira, Targeted and intracellular triggered delivery of therapeutics to cancer cells and the tumor microenvironment: impact on the treatment of breast cancer, Breast Cancer Res. Treat. 133 (2012) 61–73, https://doi.org/10.1007/s10549-011-1688-7.
[73] T. Willmer, V. Damerell, S. Smyly, D. Sims, M. Du Toit, S. Ncube, M. Sinkala, D. Govender, E. Sturrock, J.M. Blackburn, et al., Targeting the oncogenic TBX3: nucleolin complex to treat multiple sarcoma subtypes, Am. J. Cancer Res. 11 (2021) 5680–5700.
[74] N. Nohira, S. Shinji, S. Nakamura, Y. Nihashi, T. Shimosato, T. Takaya, Myogenetic Oligodeoxynucleotides as Anti-Nucleolin Aptamers Inhibit the Growth of Embryonal Rhabdomyosarcoma Cells, Biomedicines (2022) 10, https://doi.org/10.3390/biomedicines10112691.
[75] H.A. Cocker, C.R. Pinkerton, L.R. Kelland, Characterization and modulation of drug resistance of human paediatric rhabdomyosarcoma cell lines, Br. J. Cancer 83 (2000) 338–345, https://doi.org/10.1054/bjoc.2000.1273.
[76] C. Sorg, E. Schmid, N. Bortel, J. Fuchs, V. Ellerkamp, Antitumor effects of curcumin in pediatric rhabdomyosarcoma in combination with chemotherapy and phototherapy in vitro, Int. J. Oncol. 58 (2021) 266–274, https://doi.org/10.3892/ijo.2020.5155.
[77] N. Xu, Z. Hua, G. Ba, S. Zhang, Z. Liu, C.J. Thiele, Z. Li, The anti-tumor growth effect of a novel agent DMAMCL in rhabdomyosarcoma in vitro and in vivo, J. Exp. Clin. Cancer Res. 38 (2019) 118, https://doi.org/10.1186/s13046-019-1107-1.
[78] J.W. Yoon, M. Lamm, C. Chandler, P. Iannaccone, D. Walterhouse, Up-regulation of GLI1 in vincristine-resistant rhabdomyosarcoma and Ewing sarcoma, BMC Cancer 20 (2020) 511, https://doi.org/10.1186/s12885-020-06985-0.
[79] C.W. Chen, D.W. Lu, M.K. Yeh, C.Y. Shiau, C.H. Chiang, Novel RGD-lipid conjugate-modified liposomes for enhancing siRNA delivery in human retinal pigment epithelial cells, Int. J. Nanomed. 6 (2011) 2567–2580, https://doi.org/10.2147/IJN.S24447.
[80] A. Razazan, J. Behravan, A. Arab, N. Barati, L. Arabi, Z. Gholizadeh, M. Hatamipour, A. Reza Nikpoor, A.A. Momtazi-Borojeni, F. Mosaffa, et al., Conjugated nanoliposome with the HER2/neu-derived peptide GP2 as an effective vaccine against breast cancer in mice xenograft model, PLoS One 12 (2017) e0185099.
[81] M.R. Schnorenberg, S.P. Yoo, M.V. Tirrell, J.L. LaBelle, Synthesis and Purification of Homogeneous Lipid-Based Peptide Nanocarriers by Overcoming Phospholipid Ester Hydrolysis, ACS Omega 3 (2018) 14144–14150, https://doi.org/10.1021/acsomega.8b01772.
[82] X. Hu, Z. Chai, L. Lu, H. Ruan, R. Wang, C. Zhan, C. Xie, J. Pan, M. Liu, H. Wang, et al., Bortezomib Dendrimer Prodrug-Based Nanoparticle System, Adv. Funct. Mater. (2019) 29, https://doi.org/10.1002/adfm.201807941.
[83] M.G. Sun, J.F. Shi, X.Y. Li, Y. Zhao, R.J. Ju, L.M. Mu, Y. Yan, X.T. Li, F. Zeng, W. L. Lu, Targeting Epirubicin Plus Quinacrine Liposomes Modified with DSPE-PEG2000-C(RGDfK) Conjugate for Eliminating Invasive Breast Cancer, J Biomed. Nanotechnol. 11 (2015) 1339–1353, https://doi.org/10.1166/jbn.2015.2079.
[84] L. Mei, L. Fu, K. Shi, Q. Zhang, Y. Liu, J. Tang, H. Gao, Z. Zhang, Q. He, Increased tumor targeted delivery using a multistage liposome system functionalized with RGD, TAT and cleavable PEG, Int. J. Pharm. 468 (2014) 26–38, https://doi.org/10.1016/j.ijpharm.2014.04.008.
[85] X. Zhang, C. Lin, W. Chan, K. Liu, A. Lu, G. Lin, R. Hu, H. Shi, H. Zhang, Z. Yang, Dual-Functional Liposomes with Carbonic Anhydrase IX Antibody and BR2 Peptide Modification Effectively Improve Intracellular Delivery of Cantharidin to Treat Orthotopic Hepatocellular Carcinoma Mice, Molecules (2019) 24, https://doi.org/10.3390/molecules24183332.
[86] L. Xu, S. Xu, H. Wang, J. Zhang, Z. Chen, L. Pan, J. Wang, X. Wei, H. Xie, L. Zhou, et al., Enhancing the Efficacy and Safety of Doxorubicin against Hepatocellular Carcinoma through a Modular Assembly Approach: The Combination of Polymeric Prodrug Design, Nanoparticle Encapsulation, and Cancer Cell-Specific Drug Targeting, ACS Appl. Mater. Interfaces 10 (2018) 3229–3240, https://doi.org/10.1021/acsami.7b14496.
[87] T. Wei, J. Liu, H. Ma, Q. Cheng, Y. Huang, J. Zhao, S. Huo, X. Xue, Z. Liang, X. J. Liang, Functionalized nanoscale micelles improve drug delivery for cancer therapy in vitro and in vivo, Nano Lett. 13 (2013) 2528–2534, https://doi.org/10.1021/nl400586t.
[88] X. Liu, J. Xiang, D. Zhu, L. Jiang, Z. Zhou, J. Tang, X. Liu, Y. Huang, Y. Shen, Fusogenic Reactive Oxygen Species Triggered Charge-Reversal Vector for Effective Gene Delivery, Adv. Mater. 28 (2016) 1743–1752, https://doi.org/10.1002/adma.201504288.
[89] P.E. Saw, S. Kim, I.H. Lee, J. Park, M. Yu, J. Lee, J.I. Kim, S. Jon, Aptide-conjugated liposome targeting tumor-associated fibronectin for glioma therapy, J. Mater. Chem. B 1 (2013) 4723–4726, https://doi.org/10.1039/c3tb20815j.
[90] X. Wei, C. Zhan, X. Chen, J. Hou, C. Xie, W. Lu, Retro-inverso isomer of Angiopep-2: a stable d-peptide ligand inspires brain-targeted drug delivery, Mol. Pharm. 11 (2014) 3261–3268, https://doi.org/10.1021/mp500086e.
[91] G. Wang, N.Z. Mostafa, V. Incani, C. Kucharski, H. Uludag, Bisphosphonate-decorated lipid nanoparticles designed as drug carriers for bone diseases, J. Biomed. Mater. Res. A 100 (2012) 684–693, https://doi.org/10.1002/jbm.a.34002.

[92] L. Zhu, P. Kate, V.P. Torchilin, Matrix metalloprotease 2-responsive multifunctional liposomal nanocarrier for enhanced tumor targeting, ACS Nano 6 (2012) 3491–3498, https://doi.org/10.1021/nn300524f.
[93] Y. Zhang, J. Wei, J. Xu, W.S. Leong, G. Liu, T. Ji, Z. Cheng, J. Wang, J. Lang, Y. Zhao, et al., Suppression of Tumor Energy Supply by Liposomal Nanoparticle-Mediated Inhibition of Aerobic Glycolysis, ACS Appl. Mater. Interfaces 10 (2018) 2347–2353, https://doi.org/10.1021/acsami.7b16685.
[94] Y. He, L. Zhang, C. Song, Luteinizing hormone-releasing hormone receptor-mediated delivery of mitoxantrone using LHRH analogs modified with PEGylated liposomes, Int. J. Nanomed. 5 (2010) 697–705, https://doi.org/10.2147/ijn.s12129.